Rigid Body Transformations for Calibration of Prototype Fast Breeder Reactor, Steam Generator Inspection Device

S. Joseph Winston[1]([✉]), Joel Jose[1], Arun Subramaniyan[2],
S. Murugan[1], and A.K. Bhaduri[1]

[1] Indira Gandhi Centre for Atomic Research, Kalpakkam, India
{winston,joel,murugan,bhaduri}@igcar.gov.in
[2] Electrical and Electronics Department, BITS Pilani, Pilani, India
sarun2006klin@gmail.com

Abstract. Prototype Fast Breeder Reactor (PFBR) has 8 Steam Generators (SG), each with 547 tubes connecting top and bottom headers. Sodium flows in the shell side and the water/steam in the tube side. The integrity of these tubes is ascertained by periodic in-service inspection (ISI) procedures. Remote Field Eddy Current Testing (RFEC) is preferred as the SG tubes are ferromagnetic. Inverse kinematic (IK) algorithm has been developed and implemented in the motion controller for two axis system. The precise reach of tubes is often limited due to errors introduced during deployment. This paper details the use of the joint axis motor encoders to compute the error vectors through a simple forward kinematics. Singular Value Decomposition (SVD) of the correlation matrix obtained from the transformed points reveal the Euler rotation matrix which is the error rotation of the device and subsequently the translation error matrix is deduced. The sensitivity study on calibration is also carried out by inducing errors in the vertical axis error measurement. This paper details the SG inspection device calibration method which reduces cost, time and effort for the inspection.
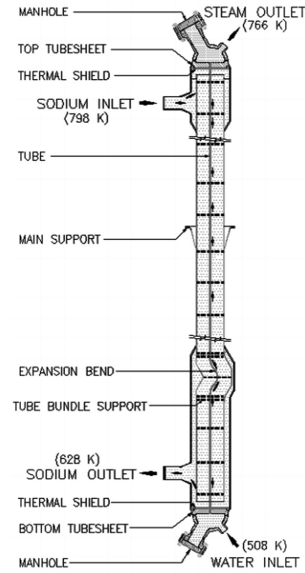
Keywords: Steam generator · Inspection system · Calibration · Robot · Correlation matrix · Singular value decomposition(SVD) · Error correction · Error sensitivity · Damped least squares (DLS) · Inverse kinematics

1 Introduction

Prototype Fast Breeder reactor (PFBR), Steam generators (SG) are 8 in numbers and have sodium in the primary shell side and water/steam in the secondary tube side. SG is about 23 m height. Figure 1 shows a typical SG. Periodic inspection of the tubes enhances the safety and also significantly reduces the operational cost through life extensions. Vision and remote Field Eddy Current Testing (RFEC) is generally carried out to qualify the tubes which separates sodium and water. Around the world SG inspection is more challenging and involves complex devices to enter and carryout the tube inspection [1]. The accessibility to the entire axial length of the tubes is only possible from the top header manhole. The inspection device has a deployment module

to lower the 2-axis robotic arm to reach closer to the tube sheet where all the tubes end at the SG top header. The two axis arm work plane is referenced to the tube sheet plane, only through long mechanical structural route which includes the mechanical assembly of the device, manhole flange, top header and the tube sheet unlike the conventional robots have a well reference fixed rigid bases. The accuracy of the inspection device depends on orientation of the deployed inspection device and also fabrication accuracies. Since the SG structure and the inspection device structures are considered to be rigid bodies, it is quite encouraging to understand that the inspection device will have a work plane and the tube sheet another. Once the inspection device is placed on the manhole for the inspection, the challenge is to remotely relate the coordinate center of the inspection device to the coordinate center of the tube sheet. This paper deals with the novel idea to use the motor encoders used for the shoulder and elbow arm

Fig. 1. Steam generator

actuation of the 2 axis system robotic arm to measure the error through a forward kinematic transform at difference tube sheet known locations and perform the Singular Value decomposition of the correlation matrix obtained from the measured to the actual theoretical values. By rigid body transformation, the rotation and the translation matrices are obtained which will be used for the correction on the fly, to reach each of the 547 tubes in the tube sheet through the Damped Least squares inverse kinematics, programmed in the motion controller. The Damped Least Squares Inverse Kinematic algorithm is implemented on the GMAS ELMO motion controller. Numerical implementation of SVD to compute the error Rotation matrix from the correlation matrix is quite expensive through a motion controller which is basically dedicated to control the axis motors. Hence, the encoder data from the controller is sent through a TCP/IP socket. Raspberry pi module receives the data and the rigid body transformation matrix is computed through the developed python code for SVD. The error Transformation matrix computed is then forwarded to the GMAS controller. In order to reach the tubes with error coordinates, the actual coordinate values are transformed through this transformation matrix and for this transformed points, the inverse kinematics is carried out to obtain the joint space variables to reach the tubes accurately. The entire process is done without reorienting the device and hence reduces significant cost, time and effort.

2 PFBR SG Inspection System-PSGIS

The complete inspection device, PSGIS has several modules performing various tasks as that of Inspection cable handling, device deployment, tube locating module, cable pushing module, Inspection system module etc. It is required to uniquely identify all the tubes and designate them with tube numbers to reference the tube inspection data against each tubes. The Tube Locator Module is a two axis robotic arm which orients to all 547 tubes of SG for pushing the RFEC probe or visual probe for inspection.

3 Tube Locator Module-TLM

The geometrical shape of TLM is designed to have the arm fit inside the deployment module which is placed into the manhole at the top header of the SG from where the system is deployed into the header. Figure 2 shows the TLM. Since the tube sheet is planar, selective compliant arm is designed and used. The kinematic move of the shoulder and elbow axes will make the end effecter i.e. the cable pushing module to orient to the tubes in the tube sheet plane. The tube number to the Cartesian coordinates with reference to the coordinate frame of the tube sheet and the inverse kinematic algorithm developed and implemented on the motion controller.
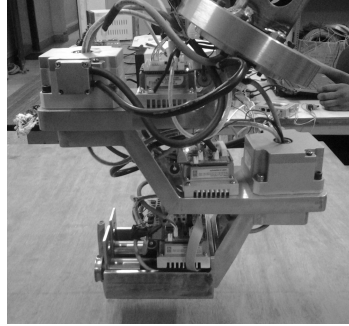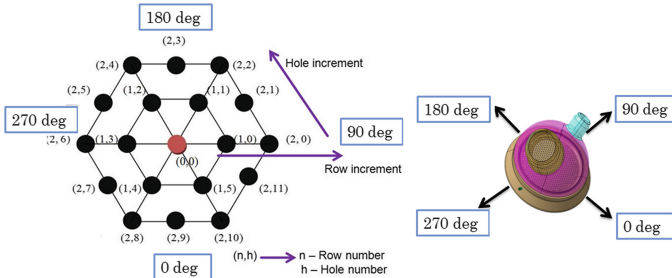

Fig. 2. Tube locator module

Fig. 3. Tube ordering scheme to reduce lookup table

Fig. 4. Dummy tube sheet & tube/hole numbering

3.1   Tube Sheet and Calibration Point Tubes/Holes- CPH

The tubes connecting the bottom header and the top header end in the tube sheet. They are in hexagonal pattern increasing in row from 0 to 14. The row 0 represents the center tube. The hole/tube number starts from 0 and runs through the hexagonal pattern as shown in Fig. 3. Figure 4 shows a dummy tube sheet and the tube ordering scheme for one small sector. Thus the tube center can be referenced from the center of the tube sheet in polar coordinate frame as shown in Eq. 1. Accordingly the tube center Cartesian coordinate is obtained from Eq. 2. This representation eliminates the storing up of all 547 tubes coordinate data in the form of lookup table into the small memory available in the motion controller. Hence, from the user input row number and tube/hole number the tube center coordinate values are computed before the IK algorithm is used to compute joint space angles for running the motors.

$$(r, \theta) = \left(a\sqrt{n^2 + h^2 - nh}, \cos^{-1}\left(\frac{a(2n - h)}{2r} \right) \right) \tag{1}$$

$$\begin{bmatrix} x \\ y \end{bmatrix} = \begin{pmatrix} r\cos\theta \\ r\sin\theta \end{pmatrix} \tag{2}$$

a -Tube pitch, 32.2 mm

Table 1.   Calibration point tubes/holes

Tube	X	Y
(11,0)	0	354.2
(11,22)	−306.746	−177.1
(11,44)	306.746	−177.1

This formulation done for 60° sector of the tube sheet to compute the coordinate values of tube center are then used to deduce for other sectors to cover all 360° by using a rotation matrix, since the tube sheet is circular symmetric in the pattern. The Calibration Point Holes (CPH), are selected on the outer region as they only can be easily identified from the actual tube sheet tube pattern. The vision camera at the end of

the elbow arm is used to locate the tubes from the tube array pattern remotely. Tube order scheme is followed to compute the coordinate values of all the 547 tubes by referring to the row number and the tube number. Table 1 shows the Calibration Point Holes and their respective coordinate values. Figure 5 shows the CPH.
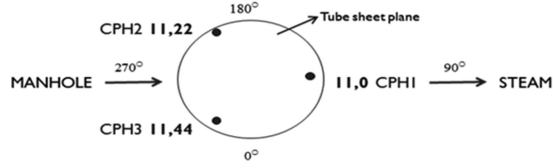
Fig. 5. Calibration point holes/tubes

3.2 Damped Least Squares (DLS) Inverse Kinematics for TLM

The joint space variables are related to the end effecter Cartesian space coordinates through the Jacobian matrix. Generally when the Jacobian matrix is a non square matrix, a pseudo inverse is carried out to perform the inversion of the Jacobian.

The forward kinematics shows the end effecter a function of joint space variables and shown in Eq. 3;

$$[e] = J[\theta] \tag{3}$$

Inverse Kinematic equation is as in Eq. 4;

$$[\theta] = J^{-1}[e] \tag{4}$$

$$J = \frac{df}{dx} = \begin{bmatrix} \frac{\partial f}{\partial x_1} \cdots \frac{\partial f}{\partial x_n} \end{bmatrix} = \begin{bmatrix} \frac{\partial f1}{\partial x1} & \cdots & \frac{\partial f1}{\partial xn} \\ \vdots & \ddots & \vdots \\ \frac{\partial fm}{\partial x1} & \cdots & \frac{\partial fm}{\partial xn} \end{bmatrix} \tag{5}$$

The Jacobian matrix is shown in Eq. 5. The pseudo inverse is named after Moore-Penrose. In all practical cases, considering the arm stability close to the singular position, the Damped Least squares (DLS) Inverse [2] is used which is shown in Eq. 6.

$$J^+ = J^T (JJ^T + \lambda^2 I)^{-1} \tag{6}$$

Where λ is a damping factor.

When the value of $\lambda = 0$, the Eq. 6 inverse will work typically as a pseudo inverse. Further, though this λ strengthens the diagonal elements of Jacobian near singular positions, it causes some errors in the end effecter tracing path which is insignificant. However this has no effect on the position reach of the TLM and is neglected.

Since the computation of the joint space variables from the Cartesian space is non-linear and the Jacobian is dependent on the pose/orientation of the TLM arm, the

solution has to be on an iterative basis in discrete steps. The two axis inverse kinematic solver has been written in python scripting for the simulation purpose and targeted on the motion controller through the programming standard IEC 61131-3 User Function Block Diagrams (UFBD) created out of Structured Text (ST) code similar to a C language syntax.

4   Errors and Calibration of the Device

The tube locator module (TLM) device is inserted through the manhole at an angle of 60° by a deployment module during inspection. The tube sheet has to be referenced from the manhole flange surface where the deployment module is mounted. The errors in the mounting of the inspection device causes a change in the orientation of the TLM with respect to the tube sheet plane. This significantly affects the performance of the device thereby missing the target tube for inspection while reaching through the Inverse Kinematics on the arm. These errors as such are not measurable through external sources as the access into the man hole is limited to the device only. Hence the exploitation of the motor encoders which are generally present in any robotic 2 axis systems to easily carry out without any additional sensor devices.

4.1   Possible Errors

The culmination of errors from the fabrication as well as mounting of the device can result in the form of combined rotation as well as translation errors. They can be well addressed as a coordinate system transformation from tube sheet plane to the device working plane.

Rotation Error. Error in mounting the device which is due to circular symmetry and may have rotation on the axis of the deployment module along the manhole or may be caused due to fabrication tolerances causing a twist of the device. Figure 6 shows the rotation error in the device.
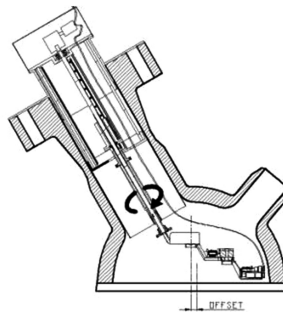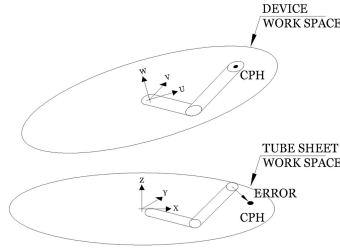

Fig. 6. Rotation error

Translation Error. Error due to device deployment module extending the deployment or falling short of the target position along with errors due to fabrication tolerances. This generates translations errors. Figure 7 shows the translation error.
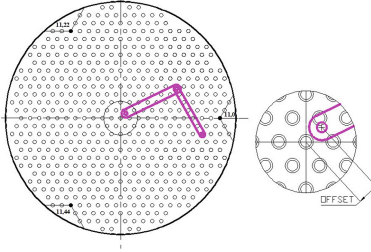
Fig. 7. Translation error

Fig. 8. Coordinate frame

4.2   Errors Represented as 3-D Right Body Transformations

The deployment module error manifests into 3 orthogonal rotations. The combined rotation cannot be decomposed to individual rotation as the matrix multiplications are noncommutative. Figure 8 shows the tube sheet and the device work plane coordinate system. It is desired to use only the Euler rotation and use the rotation elements on the combined rotation matrix for the error correction. If the θ_1, θ_2 and θ_3 are angles that represent the rotation on the axes X, Y and Z, the rotation matrices are shown as 3×3 matrix and the combined transformation matrix incorporating rotation and translation are represented as a 4×4 matrix.

Rotation error about X axis

$$
R_x = \begin{pmatrix} 1 & 0 & 0 \\ 0 & \cos\theta_1 & \sin\theta_1 \\ 0 & -\sin\theta_1 & \cos\theta_1 \end{pmatrix}
\tag{7}
$$

Rotation error about Y axis

$$R_y = \begin{pmatrix} \cos\theta_2 & 0 & \sin\theta_2 \\ 0 & 1 & 0 \\ -\sin\theta_2 & 0 & \cos\theta_2 \end{pmatrix} \tag{8}$$

Rotation error about Z axis

$$R_z = \begin{pmatrix} \cos\theta_3 & \sin\theta_3 & 0 \\ -\sin\theta_3 & \cos\theta_3 & 0 \\ 0 & 0 & 1 \end{pmatrix} \tag{9}$$

Translation error in 3 respective axes are show in Eq. 10;

$$T = \begin{pmatrix} x_0 \\ y_0 \\ z_0 \end{pmatrix} \tag{10}$$

Combined Transformation matrix which incorporates rotation and translation together in a 4 × 4 matrix is as in Eq. 11;

$$M = TR = \begin{pmatrix} r_{11} & r_{12} & r_{13} & x_0 \\ r_{21} & r_{22} & r_{23} & y_0 \\ r_{31} & r_{32} & r_{33} & z_0 \\ 0 & 0 & 0 & 1 \end{pmatrix} \tag{11}$$

4.3   Calculating the Error Transformation Matrix

The shoulder and elbow arm of TLM by virtue of interconnected rigid bodies will trace all the coordinates in its work space which is a plane. Hence tube sheet coordinate points always will get transformed respecting the rigid body transformation. Converse to the transformation of a set of tube sheet points to device work space points by transformation matrix; one has to deduce the transformation matrix from the actual tube sheet points to the device work space points considering the rigid body transformation. Hence in the present work a few selected points 3 or more which are easily identifiable from the tube sheet through vision sensors have been used to compute the actual transformation that exists between the coordinate center of tube sheet and device work plane. This transformation matrix will be used to transform all the 547 tube sheet holes to be mapped to the device coordinate frame.

Let us assume the set of coordinate points from the tube sheet, selected for the calibration be {mi}. The transformed set of {mi} points is denoted as {di} which is after the error measurement. R and T are the rotation and translation matrices that transformed {mi} points to {di}. Solving the optimal transformation that maps the set {mi} onto {di} requires minimizing a least squares error criterion [3] given by

$$\Sigma^2 = \sum_{i=1}^{N} \|di - Rmi - T\|^2 \tag{12}$$

$$\bar{d} = \frac{1}{N} \sum_{i=1}^{N} di \tag{13}$$

$$d_{ci} = d_i - \bar{d} \tag{14}$$

$$\bar{m} = \frac{1}{N} \sum_{i=1}^{N} mi \tag{15}$$

$$m_{ci} = m_i - \bar{m} \tag{16}$$

Equation 12 can be rewritten as:

$$\Sigma^2 = \sum_{i=1}^{N} (d_{ci}^T d_{ci} + m_{ci}^T m_{ci} - 2d_{ci}^T \boldsymbol{R} m_{ci}) \tag{17}$$

This equation is minimized when the term $2d_{ci}^T \boldsymbol{R} m_{ci}$ is maximized which is equivalent to maximizing Trace (RH), where H is a correlation matrix which is defined by;

$$H = \sum_{i=1}^{N} m_{ci} d_{ci}^T \tag{18}$$

If the singular value decomposition of H is given by H = U ΣV^T, then the optimal rotation matrix, R that maximizes the desired trace [4] is;

$$\boldsymbol{R} = VU^T \tag{19}$$

In order to correct the rotation matrix on some case which represents reflection rather than rotation as suggested by Umeya [5] and Kanatani [6], the rotation may be computed as;

$$\boldsymbol{R} = U \begin{pmatrix} 1 & 0 & 0 \\ 0 & 1 & 0 \\ 0 & 0 & \det(UV^T) \end{pmatrix} V^T \tag{20}$$

The optimal translation can be now deduced as follows;

$$\boldsymbol{T} = \bar{d} - \boldsymbol{R}\bar{m} \tag{21}$$

Combined error transformation matrix will be now used to transform all 547 tube center in the tube sheet before running the inverse kinematic algorithm to reach tube centers.

$$M = TR \tag{22}$$

The transformation matrix as in Eq. 22 corrects the error for the entire tube sheet for precise reach.

4.4   Error Correction Abstraction

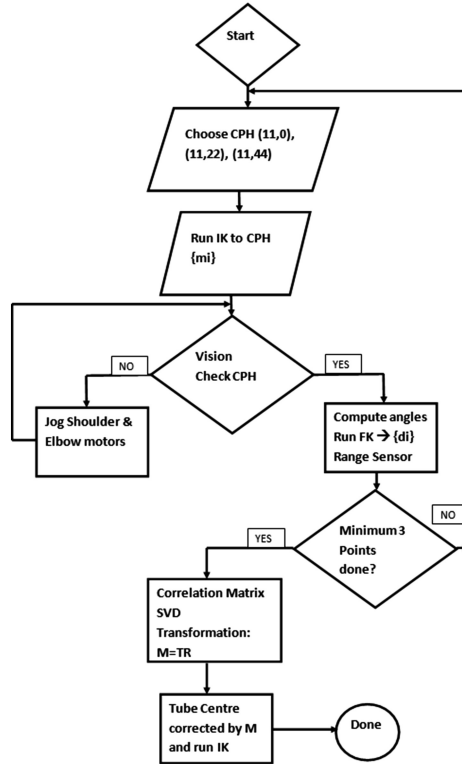Flow chart shown in Fig. 9 explains the procedure for the calibration.

Fig. 9. Calibration abstraction

5   Results and Discussion

The calibration methodology is simulated through a PC system by Python program-ming before deploying into the actual inspection device. It is to be noted that the encoders used in the arm actuators are in the order of 4 lakh counts per revolution and the position accuracy gives relatively very high order of error measurements through encoders. However if there is any error in the analog range sensor, then that induces calibration errors and hence a sensitivity study also performed to see the effect of this on calibration.

5.1   Simulated Results

To check the formulated algorithm, known angles were chosen as errors i.e. $\theta_1 = 2°$, $\theta_2 = 5°$ and $\theta_3 = 10°$ and translation errors, $(x_0, y_0, z_0) = (1,1,5)$. Figure 10 shows the schematic.
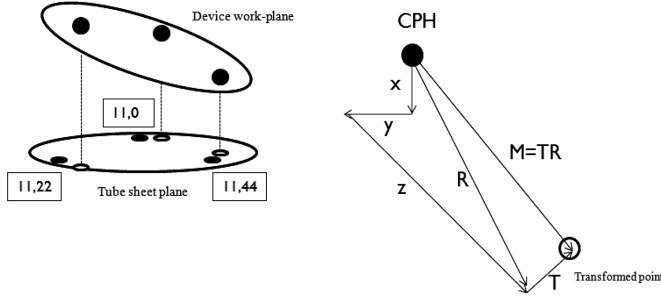
Fig. 10. Simulated error in Tube sheet and device planes

The tubes (11,0), (11,22) and (11,44) coordinate points {mi} are transformed using the transformation matrix shown in Eqs. 7, 8, 9 and the final transformed points are taken as {di}. From the original points {mi} and the transformed points {di}, the transformation matrix is computed through the rotation and translation as shown in Eqs. 20 and 21. This is compared with the same order of multiplying the 3 rotations and 3 translations. This gives the confidence on the rigid body transformation through the {mi} and {di} sets to establish the transformation matrix (Fig. 11).
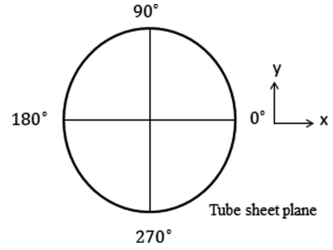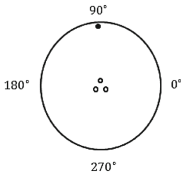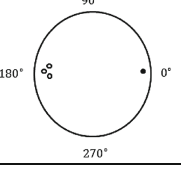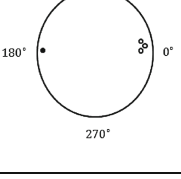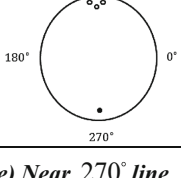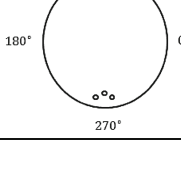

Fig. 11. Tube sheet layout

5.2   Sensitivity Analysis

Intuitively as three points are needed to fully describe a plane in $\mathbb{R}^3$, the minimum number of points needed for calibration is three. In this section, the optimum location of the three calibration points is identified. Even in the absence of mounting/fabrication errors, inaccurate measurements of the z co-ordinate of the transformed point lead to different magnitudes of error for different tubes based on the choice of number and configuration of calibration points. The motor encoder used in the TLM is devoid of backlash and hence the Cartesian co-ordinates in tube sheet plane can be measured accurately through a forward kinematic procedure using the joint space angular positions.

Table 2. Point pivoting

Location	Tube	% Error	Error mm	Max. Error Tube
a) Near center (1,0), (1,2), (1,4)		5	0.21	(13,2)
	(1,0)	15	1.91	(13,2)
		50	19.82	(13,2)
b) On $180°$ line (10,15), (11,16), (11,17)		5	1.14	(14,61)
	(10,15)	15	10.09	(14,61)
		50	92.15	(14,61)
c) Near $0°$ line (10,45), (11,49), (11,50)	(10,45)	5	1.14	(14,19)
		15	10.09	(14,19)
		50	92.15	(14,19)
d) Near $90°$ line (11,0), (11,1), (11,65)	(11,0)	5	3.62	(13,37)
		15	30.78	(13,37)
		50	213.77	(13,37)
e) Near $270°$ line (11,32), (11,33), (11,34)	(11,33)	5	3.62	(13,2)
		15	30.78	(13,2)
		50	213.77	(13,2)

Table 3. Line Pivoting
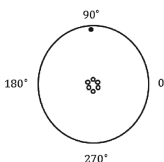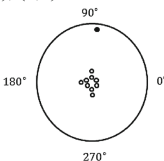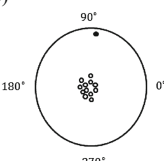
Location	Tube	% Error	Error mm	Max. Error Tube
a) Vertical line (2,3), (11,0), (11,33)		5	0.17	(14,61)
	(2,3)	15	1.52	(14,62)
		50	16.04	(14,65)
b) Horizontal line (1,0), (10,15), (10, 45)		5	0.49	(13,37)
	(1,0)	15	4.39	(13,37)
		50	41.92	(13,37)
c) Diagonal line (1,5), (9,6), (9,33)	(1,5)	5	0.51	(14,33)
		15	4.59	(14,33)
		50	43.61	(14,33)

In the simulation, it is chosen a reasonable error in the z axis measurement. When the z-axis corresponding to all the three calibration points have the same error in measurement, the device work-plane is simply translated in the z-direction by the same amount and the choice of calibration points has no effect. The worst case arises when a single calibration point is incorrectly measured (or has a different error magnitude compared to the other two points).

It is found that when the three points are arranged so as to resemble an equilateral triangle of maximum area, the sensitivity of the error is minimum. An alternative to the optimum configuration is choosing a cluster of nearby tubes 6 to 12 numbers on the tube sheet plane for calibration. Table 2 shows the set of points selected close to each other in different locations, near center and at other angular directions.

The tube sheet tube pitch is 32.2 mm and hence errors are simulated as a percentage of this. Table 2 shows that 5 %, 15 % and 50 % errors are applied on tube (1,0) and

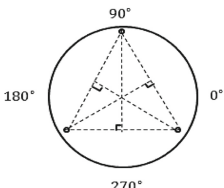**Table 4.** More points chosen for calibration

No. of tubes	Location	Tube	% Error	Error mm	Max. Tube Error
6	**Near the centre** (1,0), (1,1), (1,2), (1,3), (1,4), (1,5)		5	0.0537	(13,2)
		(1,0)	15	0.4821	(13,2)
			50	5.2574	(13,2)
9	**Near the centre** (1,0), (1,1), (1,2), (1,3), (1,4), (1,5), (2,0), (2,3), (2,6)		5	0.0047	(14,78)
		(1,0)	15	0.0422	(14,78)
			50	0.4685	(14,78)
12	**Near the centre** (1,0), (1,1), (1,2), (1,3), (1,4), (1,5), (2,0), (2,2), (2,3), (2,4), (2,5), (2,6)	(1,0)	5	0.00393	(14,75)
			15	0.0354	(14,75)
			50	0.3929	(14,75)

this yields a maximum error at tube location (13,2) such as 19.8 mm for 50 % z axis measurement. Similarly at other locations clustered points give more errors as seen in the same table.

If the selected calibration points are close to one another, a sort of point pivoting takes place which shows error magnification proportional to the radial distance of other tubes from the clustered calibration point tubes.

Table 3 shows a line pivoting when the calibration points are so chosen along a straight line or close to a straight line. The vertical line pivots, horizontal line pivots and the pivotal line where the calibration points are chosen clearly indicate the

Table 5. Optimal selection of calibration point tubes

Location	Tube	% Error	Error mm	Max. error Tube
Equilateral triangle (11,0), (11,22), (11,44)		5	0.002	(13,2)
	(11,0)	15	0.016	(13,2)
		50	0.177	(13,2)

calibration errors are magnified normal to the distance from the line as seen from Fig. 12 which shows the error vector.

Table 4. shows the calibration errors when more number of calibration points are chosen. The case study was done for 6, 9 and 12 number of calibration points chosen and an error of 5 %, 15 % and 50 % applied to a particular tube on the z axis. Significant reduction in the calibration error noticed when more calibration points are chosen (Fig. 13).

When the points chosen for calibration are widely spread apart, typically forming an equilateral triangle, then even with less number of calibration points (i.e. with the minimum number of points) the errors are found to be significantly reduced as seen from Table 5. This strengthens the argument of using the calibration points holes (11,0), (11,22) and (11, 44) a good choice. These tubes are also easily identifiable from the tube sheet pattern. Figure 14 shows the vector plot of the calibration error considering 3 points which form an equilateral triangle.
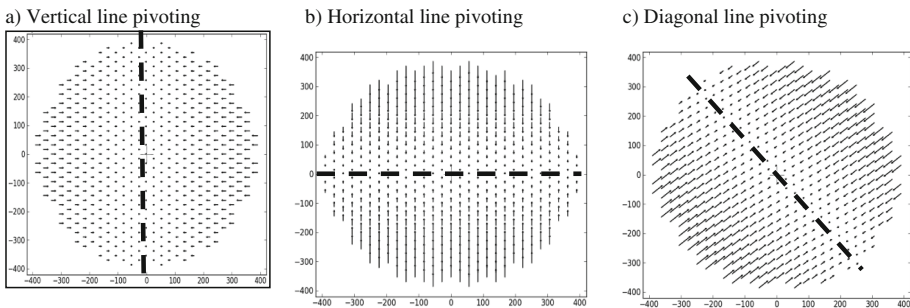
Fig. 12. Calibration points chosen along a line which causes line pivoting
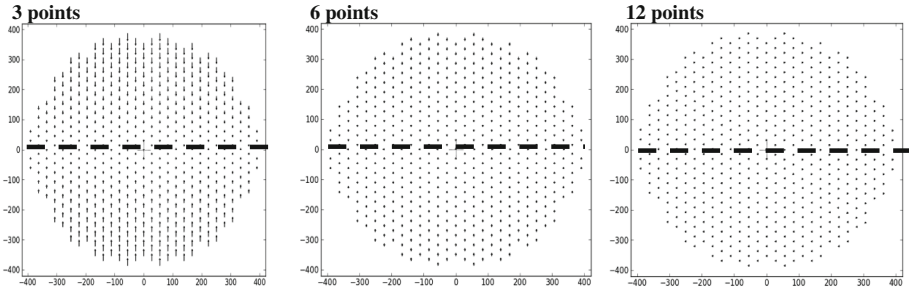
**Fig. 13.** More calibration points reduces error
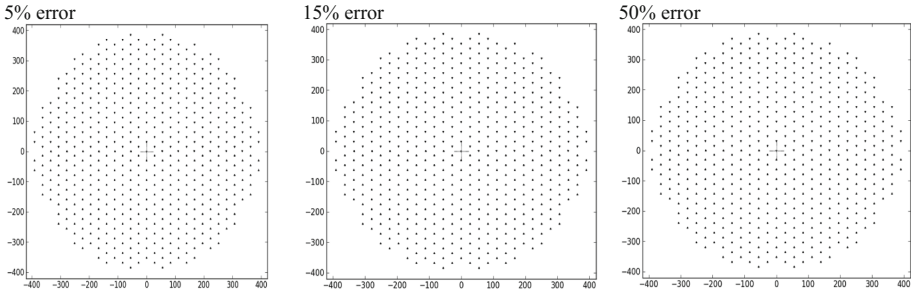
Fig. 14. Choosing widely separated calibration points reduces calibration errors

6   Implementation

It is quite expensive to implement the numerical SVD scheme into the tiny motion controllers which is already running motion controls with highest priority. Also the numerical SVD techniques are far different from the canonical way of theoretical computations of SVD [7, 8]. However an attempt was made implementing the Jacobi rotation numerical method [9] and found to be controller intensive. To implement in the inspection device, it was programmed in the motion controller to make available the axis encoder data on a TCP/IP port. Figures 15 and 16 shows the TLM and calibration mockup facility developed to ascertain the validity of the calibration parameter.

A Raspberry pi system with python is wirelessly connected to the motion controller to acquire the encoder data and populate the {di} set of points after the jogging of the motors correcting the errors manually using a vision system. Figure 17 shows the schematic layout of the implemented system.
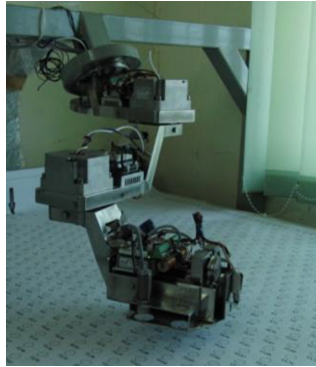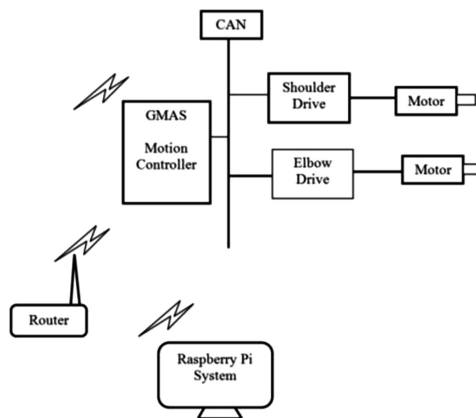
Fig. 15. TLM on calibration table
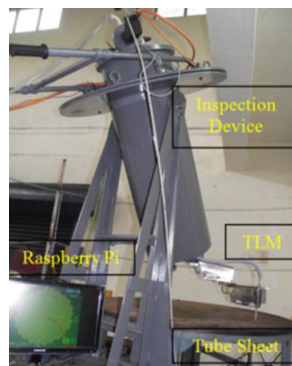
Fig. 16. Calibration setup of the complete device including TLM

Fig. 17. Raspberry Pi module for SVD

7 Conclusion

Steam Generator inspection device requires correlating the device work and the tube sheet coordinate frame. A calibration methodology has been evolved and implemented using the SVD decomposition of the correlation matrix obtained from the theoretical tube centers to the measured deviated position of the tube center. The errors are unavoidable during the mounting of the device on the manhole for SG tube inspection and this methodology significantly reduces cost, time and effort. Also it reduces the fabrication cost by relaxing the tolerances there by correcting all the rotation and translation errors during calibration. The motor axis encoders are used to measure planar errors through forward kinematics along with the range sensor. Simulation of the rigid body transformation parameter estimation done using python scripting language. The implementation is done on the SG inspection device arm to correct the errors on the fly without re-orienting the device. This may be applicable to similar devices that need calibration when reoriented on the base of the robotic system.

References

1. Obrutsky, L., Renaud, J., Lakhan, R.: Steam generator inspections: faster, cheaper and better, are we there yet? In: IV Conferencia Panamericana de END, Buenos Aires–Octubre 2007
2. Ross, S.R.: Introduction to inverse kinematics with jacobian transpose, pseudoinverse and damped least squares method. Department of Mathematics, University of California, San Diego, 7 October 2009
3. Eggert, D.W., Lorusso, A., Fisher, R.B.: Estimating 3-D rigid body transformation: a comparison of four major algorithms. Mach. Vis. Appl. **9**(5), 272–290 (1997)
4. Challis, J.H.: A Procedure for determining rigid body transformation parameters. Biomechanics **28**, 733–737 (1995)
5. Umeyama, S.: Least Squares estimation of Transformation parameters between two point patterns. IEEE Trans. Pattern Anal. Mach. Intell. **13**, 376–380 (1991)
6. Kanatani, K.: Analysis of 3-D rotation fitting. IEEE Trans. Pattern Anal. Mach. Intell. **16**, 543–549 (1994)
7. Kalman, D.: A singular Value Decomposition: The SVD of a Matrix. The American University, Washington DC 20016, 13 February 2002
8. Wei, S., Lin, Z.: Accelerating iterations involving eigenvalue or singular value decomposition by block lanczos with warm start. Microsoft Technical Report # MSR-TR-2010–162
9. Golub, G.H., Van Loan, C.F.: Matrix Computations. The John Hopkins University Press, Baltimore (1996)